

Bimodal grain size distributions in UFG materials produced by SPD – their evolution and effect on the fatigue and monotonic strength properties

M. Korn¹, R. Lapovok², A. Böhner¹, H. W. Höppel¹, H. Mughrabi^{1*}

¹University of Erlangen-Nürnberg, Department of Materials Science and Engineering, Institute I, Martensstr. 5, 91058 Erlangen, Germany

²Monash University, Materials Engineering, Building 19, Clayton 3800, Australia

Received 26 July 2010, received in revised form 3 September 2010, accepted 3 September 2010

Abstract

In ultrafine-grained (UFG) materials produced by severe plastic deformation (SPD) techniques such as ECAP (equal channel angular pressing), bimodal grain size distributions have been observed under different circumstances, for example shortly after ECAP, after rest or anneal and/or after mild cyclic deformation at rather low homologous temperature. It has been shown that the mechanical monotonic and fatigue properties of some UFG materials can be modified (sometimes enhanced) by introducing a bimodal grain size distribution by a mild annealing treatment which leads, in some cases, to a good combination of strength and ductility. Here, the conditions under which bimodal grain size distributions evolve by (adiabatic) heating during ECAP and during subsequent annealing or cyclic deformation will be explored, and the effects on the mechanical properties, as studied by the authors and as reported so far in the literature, will be reviewed and discussed. In particular, the role of temperature rise during ECAP will be considered in some detail.

Key words: UFG, ultrafine-grained microstructure, bimodal grain size distribution, fatigue life enhancement, grain coarsening, ECAP temperature rise

1. Introduction

Since more than a decade, bulk ultrafine-grained (UFG) metals with grain sizes below one micron can be produced by different severe plastic deformation (SPD) techniques [1–3]. Among the latter, equal channel angular pressing (ECAP) is most widespread. Because of their extraordinary strength properties, compared to those of conventional grain size (CG) materials, UFG metals and alloys produced by ECAP have attracted much attention. However, since the ECAP-processed material is heavily predeformed, its grain microstructure is thermally metastable or even unstable and prone to undergo more or less severe microstructural changes, involving grain boundary migration and (local) grain coarsening [1, 4–9] even at moderate temperatures. Thus, bimodal grain size distributions, consisting of regions with coarsened grains

amidst the original UFG grain structure, have been observed repeatedly in bulk ECAP-processed UFG materials, e.g., copper, nickel and α -brass under different, frequently not well-defined circumstances, for example

- after mild cyclic strain-controlled deformation at room temperature [6, 9, 10–14], whereas a similar effect was almost absent after stress-controlled fatigue [12],
- after long-time rests at room temperature [8, 9] or short-time anneals at higher temperatures [5, 6, 11, 12, 15], and
- shortly after ECAP-processing, probably caused by concomitant temperature rise [9, 16, 17].

In OFHC copper, subjected to another SPD technique, namely 7 cycles of accumulated roll bonding (ARB), a related similar bimodal grain size distribution, referred to by the authors as a “composite micro-

*Corresponding author: tel.: +49 9131 8527482; fax: +49 9131 8527504; e-mail address: mughrabi@ww.uni-erlangen.de

structure” was observed [18]. Furthermore, it should be noted that grain coarsening has also been observed to occur during stressing/deformation of truly nanocrystalline (NC) materials with grain sizes below 100 nm at moderate or even low temperatures [19–21]. Aside from their considerably smaller grain sizes, NC materials are usually distinct from UFG materials, being produced not by SPD-techniques, but in quite different ways (e.g. physical vapour deposition, electrodeposition). Thus, the initial microstructural states differ in characteristic manner, in particular with respect to dislocation content and internal stresses. Nonetheless, in both cases driving forces to reduce the grain boundary energy exist and can promote grain coarsening.

In some cases, UFG materials containing an initially bimodal grain size distribution have been found to exhibit enhanced fatigue [12, 22–24] and monotonic [25, 26] strength properties. This has been attributed to the combined effects of the larger grains which provide ductility by work hardening and the very small grains that enhance the strength. Thus, efforts have been made to deliberately introduce bimodal grain size distributions by suitable means. In the case of ECAP-processed UFG materials, this is possible by appropriate annealing treatments of the ECAP-processed material [6, 11, 23, 24]. Powder technological techniques involving blending of UFG and CG powders, pressing and extrusion represent a completely different approach to produce bimodal grain structures in UFG materials to achieve good strength and ductility [27, 28]. The present work is essentially confined to studies on UFG materials produced by ECAP or related SPD-techniques.

The effect of bimodal grain size distributions on the strength properties seems to have been generally beneficial in the cases of monotonic deformation so far investigated [25, 26]. On the other hand, the effect on the fatigue strength has been beneficial in some cases [11, 23, 24] but not in others [6, 9, 24]. The present work is based on an earlier shorter communication [9]. The aim is to present and discuss in more detail some new results, to identify and clarify the conditions under which bimodal grain structures evolve in SPD-processed material and to discuss their effects on the mechanical properties, with a special emphasis on the fatigue performance of UFG materials.

2. Evolution of bimodal grain size distributions during strain- and stress-controlled fatigue

In an early study on UFG copper (99.98 %) by Agnew and Weertman [10], an interesting observation was made, namely that, during fatigue in strain control at room temperature (RT), strong cyclic softening

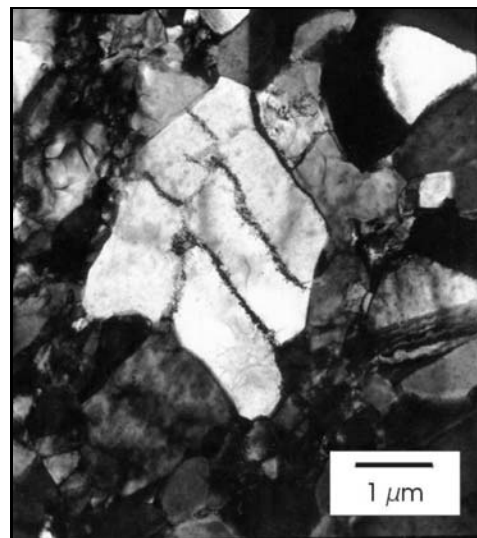


Fig. 1. High-purity UFG copper. TEM micrograph of bimodally coarsened grain structure after fatigue ($\Delta\varepsilon_{p1} = 5 \times 10^{-4}$, RT). From [11].

ing occurred. At the same time, it was noted that the originally strongly ECAP-hardened and more or less homogeneous UFG grain structure had undergone a marked coarsening in locally confined regions, whereas the original UFG microstructure was retained in the remaining regions. Similar results were obtained on fatigued high-purity (99.99 %) UFG copper [11, 12], in which clearly bimodal grain size distributions were found, and in similar work on fatigued high purity (99.99 %) nickel [13]. Figure 1 shows as an example a TEM micrograph of the bimodal grain structure observed in UFG copper after fatigue. It follows that, in the as-ECAP-processed UFG copper, the grain structure is microstructurally unstable at RT, i.e. at a rather *low homologous temperature* of roughly 0.2. The process of local grain coarsening during deformation has been identified as thermally activated temperature- and strain-rate-dependent dynamic recrystallization/grain coarsening [12]. It is worthwhile to emphasize again the remarkable finding that, in stress-controlled fatigue of high-purity UFG copper, almost no cyclic softening occurred, and local grain coarsening was almost negligible [11, 12].

The migration of grain boundaries is believed to play a key role in the coarsening process. Contrary to the long-held belief that only low-angle grain boundaries can move under the action of an applied stress, it is clear from the pioneering work of Winning et al. [29] that this is also true for high-angle grain boundaries. Evidence to this effect has also been observed and elaborated more recently in studies on strained nanocrystalline materials [19–21]. On the other hand, in the absence of an external stress, the driving force to reduce the grain boundary area, viz. energy, re-

mains nonetheless effective and can lead during annealing to local grain boundary migration and thus to bimodal grain coarsening. Since impurities impede the migration of grain boundaries, cyclic softening related to bimodal grain coarsening would normally be expected to be suppressed or less marked in less pure material [6, 12]. Thus, in seeming agreement with this expectation, the Brno group reported that there was no bimodal grain coarsening after fatigue of copper of commercial purity at RT [30]. However, these fatigue tests had been conducted in stress control. Only very recently, the same authors performed strain-controlled fatigue tests on the same material and now found cyclic softening and bimodal grain coarsening [31], comparable to the results obtained in the earlier work on high-purity UFG copper [11, 12]. Thus, in fatigue tests on UFG copper of different purities at RT, no appreciable effect of purity with regard to the occurrence of bimodal grain coarsening seems to exist. Nonetheless, it can easily be imagined that, at a somewhat lower temperature, cyclic softening, accompanied by bimodal grain coarsening, would still occur in the material of higher purity but not in the less pure material. Specific tests to check this hypothesis are desirable.

3. Fatigue lives of CG and UFG materials

Good fatigue performance is one of the most important mechanical properties expected from new structural materials. Thus, UFG materials should exhibit, in addition to their remarkable monotonic strength and ductility properties, good fatigue resistance, comparable to or better than that of CG material. However, in the early fatigue studies on UFG copper this expectation was not borne out clearly in a general sense [10, 11, 32, 33]. For a more detailed discussion, it is expedient to review briefly fatigue life behaviour in the High Cycle Fatigue (HCF) and Low Cycle Fatigue (LCF) ranges [33, 34]. In the HCF range, fatigue lives are most frequently displayed in so-called Wöhler or S - N plots of stress amplitude $\Delta\sigma/2$ vs. numbers of cycles to failure, N_f . In addition, HCF life data are also frequently represented in terms of the Basquin relation:

$$\frac{\Delta\sigma}{2E} = \frac{\Delta\varepsilon_{el}}{2} = \frac{\sigma'_f}{E}(2N_f)^b. \quad (1)$$

On the other hand, fatigue lives in the LCF regime are commonly described in terms of the Coffin-Manson relationship:

$$\frac{\Delta\varepsilon_{pl}}{2} = \varepsilon'_f(2N_f)^c. \quad (2)$$

Here, $\Delta\varepsilon_{el}/2$ is the elastic strain amplitude, $\Delta\varepsilon_{pl}/2$ is the plastic strain amplitude, E is Young's modulus;

σ'_f and ε'_f are the fatigue strength and fatigue ductility coefficients, respectively, and b and c are the fatigue strength and the fatigue ductility exponents, respectively. The exponents b and c are negative and assume typical values of $b \approx -0.1$ and $c \approx -0.5$ in many cases [34, 35]. It follows from the above that *ductile* materials with high ε'_f are expected to exhibit good LCF resistance, whereas *strong* but less ductile materials with high σ'_f have good HCF strength.

Now, since the early work on fatigued UFG copper [10–12, 32] it has always been found, also in the case of other UFG metals [23, 36], that the fatigue lives are *larger*, compared to those of CG copper, when plotted in a Wöhler (S - N) plot but *shorter* when plotted in a Coffin-Manson plot. As proposed earlier [33, 37], this behaviour is most easily understood by considering the fatigue lives of UFG and CG materials in a so-called total strain fatigue life diagram. The total strain is given by $\varepsilon_t = \varepsilon_{pl} + \varepsilon_{el}$. Making use thereof, the total strain fatigue life relationship is obtained by adding the expressions for the Wöhler S - N and the Coffin-Manson laws, compare [37]:

$$\frac{\Delta\varepsilon_t}{2} = \frac{\Delta\varepsilon_{el}}{2} + \frac{\Delta\varepsilon_{pl}}{2} = \frac{\sigma'_f}{E}(2N_f)^b + \varepsilon'_f(2N_f)^c. \quad (3)$$

In the asymptotic limit of large plastic strain amplitudes ($\Delta\varepsilon_{pl} \gg \Delta\varepsilon_{el}$), this expression reduces to the Coffin-Manson relation, whereas, at very low amplitudes ($\Delta\varepsilon_{pl} \ll \Delta\varepsilon_{el}$), it becomes similar to the Wöhler-type S - N relation between stress amplitude and number of cycles to failure.

Comparing UFG and annealed CG materials, it is now straightforward to *classify ECAP-processed heavily pre-deformed materials as strong materials and CG materials as ductile materials*. Accordingly, it will be expected that, in the total strain fatigue life diagram, UFG materials will exhibit longer fatigue lives in the strength-controlled HCF regime but shorter fatigue lives in the ductility-governed LCF regime with the effect that *the total strain fatigue life diagrams of both materials will be expected to intersect*. All of these features of the expected fatigue behaviour are in accordance with observation [10–12, 24, 32, 36].

4. Introduction of bimodal grain size distributions by annealing to enhance the fatigue properties

4.1. Enhancement of fatigue lives in UFG copper by an annealing treatment resulting in a bimodally coarsened grain structure

As explained earlier, it is well known that good LCF performance requires a sufficiently high ductility [34, 35]. Thus, in view of the lowered ductility

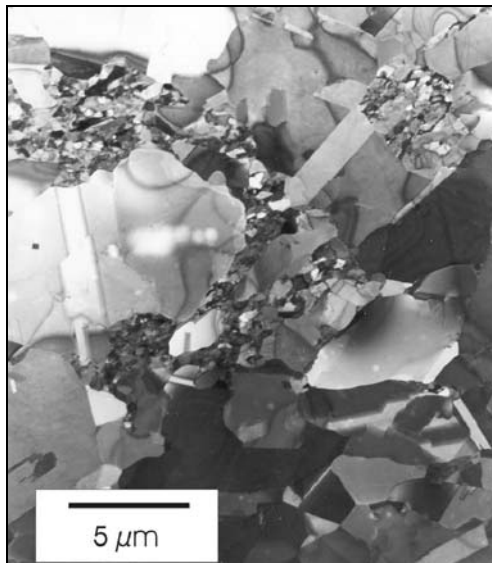


Fig. 2. High-purity UFG copper. TEM micrograph of “optimally” bimodally coarsened grain structure after annealing (170°C, 2 h). From [11].

of the strongly ECAP-hardened UFG material, the rather unsatisfactory LCF fatigue performance, as revealed in a Coffin-Manson plot, is understandable. In an attempt to remedy this deficiency, Höppel et al. [11, 12], more than 10 years ago, compare also [6], subjected their UFG copper of high purity (99.99 %) to a mild annealing treatment in order to enhance the ductility at the expense of a moderate loss of strength. In a systematic search for the most suitable annealing treatment with respect to enhancing fatigue life, a 2 h anneal at 170°C was found to be optimal. In the annealed material, a bimodal grain size distribution was found, with coarse grains of some μm grain size embedded in the original UFG grain structure. With increasing annealing time, the volume fraction of coarse grains increased. Figure 2 shows, as an example, a TEM micrograph of the annealed UFG copper with the optimal bimodal grain size distribution [11]. It should be noted that in this case the interiors of the coarsened grains are almost free of dislocations, in marked contrast to the case of the fatigue-induced bimodally coarsened grain structure in which, just as in CG material, typical wall/cell structures developed in the larger grains (Fig. 1). The annealed bimodally coarsened UFG copper exhibited a remarkable enhancement of fatigue lives by a factor of 7 in the Coffin-Manson plot and an overall excellent fatigue performance, implying that the optimal bimodal grain size distribution provides a good compromise between fatigue strength and ductility.

This result suggested that the introduction of a bimodal grain structure could be a general measure to markedly improve the overall mechanical proper-

ties of UFG materials, as had also been shown a little later in the case of monotonic deformation [25, 26]. However, so far, it has not been possible to achieve similarly large enhancements of fatigue performance in UFG materials other than UFG copper [11, 33, 38–40]. Based on the strong similarities between the cyclic deformation and annealing behaviours of UFG copper and UFG nickel that were mentioned before, it appears very probable that the (LCF) fatigue lives of UFG nickel can also be improved markedly by the introduction of a bimodal grain size distribution by an annealing treatment.

4.2. Fatigue behaviour of ECAP-processed copper with unintentional initial bimodal grain size distribution

In order to compare the fatigue behaviours of UFG copper specimens produced by ECAP without and with *back pressure* (BP) of 150 MPa [41], an experimental study was conducted on such specimens and on companion CG specimens. Details of ECAP-processing were as follows: 12 passes, route B_c, ECAP speed: 5 mm s⁻¹. The hope was that the UFG copper produced with ECAP and BP would have the most fatigue-resistant grain microstructure. The results of this study were interesting and puzzling. Since that time, it was thought that the UFG grain structure of commercial purity UFG copper would be stable at RT [30], no precautions were taken to store ECAP-processed material at low temperatures. For this reason, the ECAP-processed material rested for months at RT before the fatigue tests. Then, after the fatigue tests had been started, the authors were aroused by an unusually large scatter of the fatigue lives observed. Subsequent inspection of the initial grain microstructure revealed more or less large regions of a bimodally coarsened grain distribution in the initial UFG grain structure, inherited in all probability from deformation-induced heating during ECAP (see Section 7) and/or from further coarsening during resting at RT after ECAP (Section 5).

The fatigue life data obtained in this study are displayed in Figs. 3a,b in a Wöhler *S-N* and in a Coffin-Manson plot, respectively, with some other published data of fatigue lives $N_{f,UFG}$ of UFG copper [10, 11]. Within the scatter, the fatigue lives $N_{f,bimodal}$ of the bimodally coarsened copper specimens that had been ECAP-processed with/without BP were similar. It should be noted that, while there is a broad scatter band, all the data of one particular type of material can be pooled together, showing that the fatigue lives $N_{f,bimodal}$ and the fatigue lives of the annealed ECAP-processed specimens [11, 12] were larger than the fatigue lives $N_{f,CG}$ of the CG material, not only in the Wöhler *S-N* but also in the Coffin-Manson plot. This quite remarkable enhancement of fatigue performance

Table 1. Parameters obtained in fit of fatigue life data of ECAP/bimodal and CG copper to total strain fatigue life relationship. The related effects of enhancements or reductions of fatigue life of the ECAP/bimodal specimens with respect to the fatigue performance of the CG material are indicated by the inserts $N_f \uparrow$ and $N_f \downarrow$, respectively

Cu structure	σ'_f (MPa)	b	ε'_f	c
CG	514.5	-0.14	0.60	-0.6
ECAP/bimodal	514.5	-0.12 $N_f \uparrow$	0.53 $N_f \downarrow$	-0.53 $N_f \uparrow$

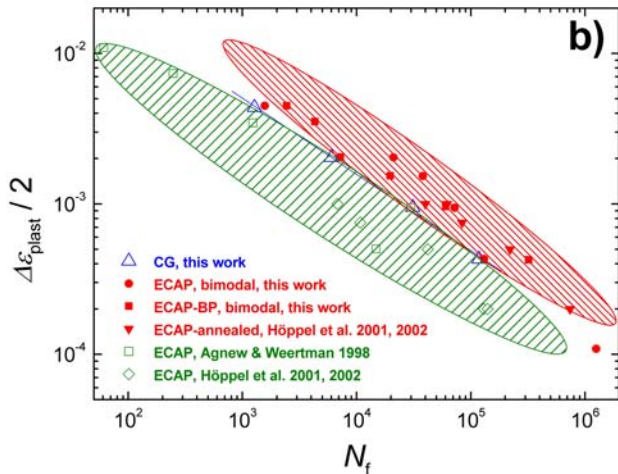
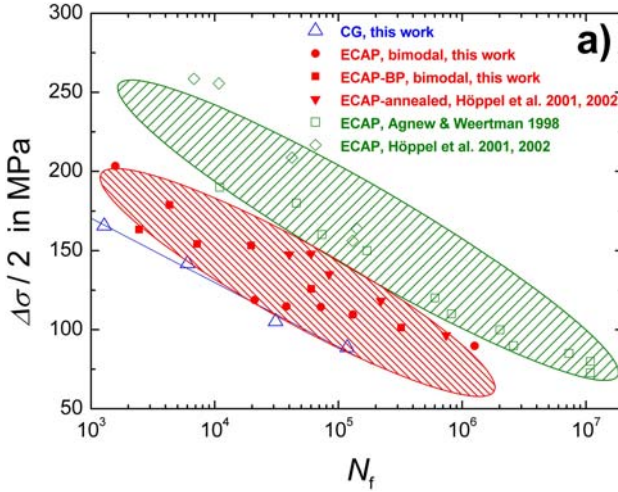


Fig. 3. Fatigue life data of commercial purity UFG copper, processed by ECAP without and with back pressure (ECAP-BP). a) Wöhler (S - N) plot, stress amplitude $\Delta\sigma/2$ vs. number of cycles to failure, N_f , showing roughly: $N_{f,CG} \leq N_{f,bimodal} \leq N_{f,UFG}$. b) Coffin-Manson plot, plastic strain amplitude $\Delta\varepsilon_{pl}/2$ vs. N_f , showing roughly: $N_{f,UFG} \leq N_{f,CG} \leq N_{f,bimodal}$. Here, $N_{f,UFG}$ refers to the fatigue lives from [10, 11]. From [9].

is similar to the improvement achieved in the case of high-purity UFG copper by annealing, discussed in Section 4.1. In the present case, the initial bimodally coarsened grain structure of admittedly ill-defined origin obviously had a beneficial effect. In order to

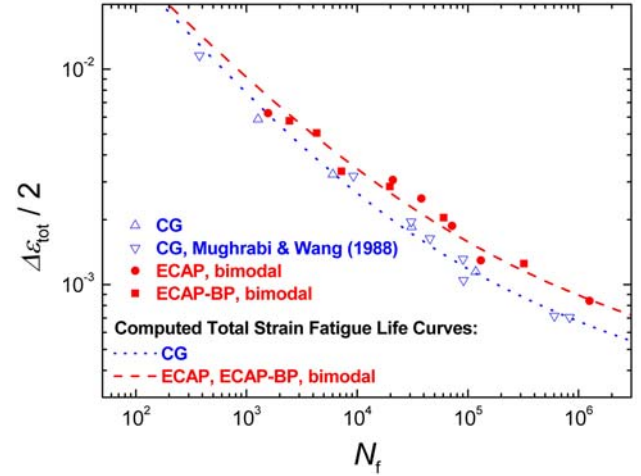


Fig. 4. Total strain fatigue life data of bimodally coarsened ECAP-processed (with and without BP) commercial purity copper. The same data as in Figs. 3a,b. Comparison with data of CG copper.

assess the reasons behind this behaviour in more detail, the fatigue life data of the ECAP-processed copper and of the CG counterparts, supplemented with very similar CG data from an earlier study [42], are shown in a total strain fatigue life plot in Fig. 4. All ECAP/bimodal and all CG fatigue life data were lumped together into one set of data each. By fitting the two sets of data to the total strain fatigue life relationship according to Eq. (3), the relevant constants σ'_f , ε'_f , b and c were obtained for both sets of data, as listed in Table 1. Using these values, the total strain fatigue life curves were computed according to Eq. (3) and plotted in the figure. The interesting result is that, over the whole life range investigated, the bimodally coarsened UFG copper exhibited markedly longer fatigue lives than the CG copper. The detailed reasons follow from an inspection of the parameters listed in Table 1. It is interesting that the fatigue strength coefficient σ'_f is similar for the ECAP/bimodal and the CG material. In the entire range investigated, the fatigue lives of the ECAP/bimodal material are larger than those of the CG material. However, at very large amplitudes, viz. very short fatigue lives of the order $N_f < 100$, the two fatigue life curves would probably intersect as a result of the fact that the fatigue

ductility coefficient ε'_f is larger for the CG than for the ECAP/bimodal material. The latter, by itself, would be beneficial for the LCF life of the CG material. However, both the fatigue ductility exponent c and the fatigue strength exponent b are smaller in magnitude in the case of the ECAP/bimodal material, thus enhancing both its LCF and its HCF life with respect to that of the CG material in the range investigated. Obviously, this latter effect outweighs the influence of the larger fatigue ductility of the CG material, at least in the range investigated.

This result confirms the beneficial effect of bimodal grain coarsening in the case of UFG copper. Beyond that, the result is reminiscent, with respect to fatigue, of what Valiev et al. referred to as the *Paradoxon of strength and ductility in metals processed by severe plastic deformation* [43], implying that, in severely plastically deformed metals, both the strength and the ductility can be enhanced. The impressive results shown here for fatigued ECAP-processed copper, with superior fatigue resistance in LCF and HCF, come close to the case of Valiev's paradoxon.

5. Evolution of bimodal grain size distributions during ageing at room or higher temperatures or during ECAP

5.1. General – the special case of UFG aluminium compared with UFG copper or UFG nickel

It has been noted that it is not always possible to obtain bimodal grain structures by annealing [24, 38–40]. In bulk SPD-processed UFG metals, bimodal grain size distributions have so far only been encountered or produced readily by annealing in the case of nickel [5], copper and α -brass [24, 36, 38, 40], whereas UFG aluminium appears to be a different more complex case. Thus, considerable efforts to introduce a bimodal grain structure in commercial purity UFG aluminium by annealing failed [38], since grain coarsening always occurred in a more or less homogeneous manner. Supporting evidence comes from the observation that, in both UFG high-purity copper and UFG commercial purity aluminium, grain coarsening was noted after a rest of some months (up to a year) at RT after ECAP-processing. However, whereas a *typical bimodal grain size structure developed in the case of UFG copper, a more or less homogeneously coarsened grain structure was observed in UFG aluminium*, as noted previously above.

The crucial factor seems to be the competition between the driving forces for recovery and recrystallization and the different kinetics, as illustrated schematically in Fig. 5 [24, 38], adapted from standard textbooks. In the case of aluminium, rapid initial recov-

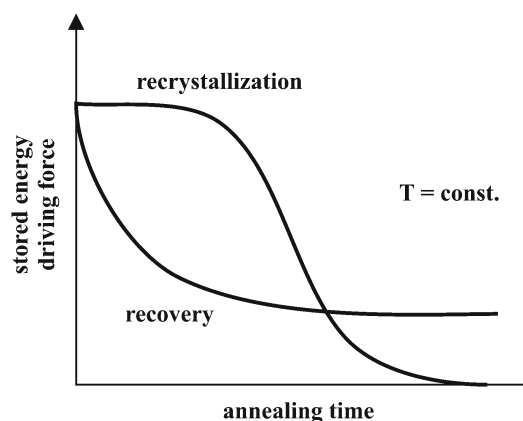


Fig. 5. Schematic illustration of the different driving forces and kinetics of recovery and recrystallization. From [24, 38].

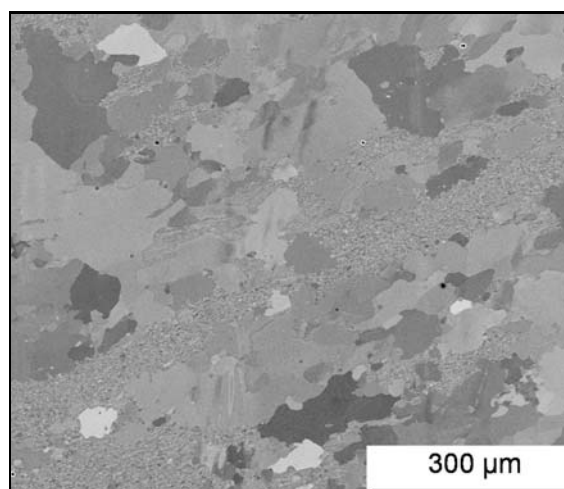


Fig. 6. Bimodal grain size distribution in 99.999 % aluminium after ECAP (8 passes, B_c). SEM micrograph. Courtesy of J. May [16].

ery is favoured by the high stacking fault energy [44]. Then, not enough driving force is left for subsequent recrystallization. This is probably the explanation why bimodal grain structures are not readily formed in annealed *commercial purity* UFG aluminium. In addition, some indirect evidence suggests that bimodal grain coarsening may occur more readily in *high-purity* aluminium. Thus, bimodal grain structures have been observed in high-purity aluminium both after (cyclic) high pressure torsion (HPT) [45] and also after ECAP-processing at RT [16, 17]. Figure 6 shows an example of a bimodal grain size distribution in ECAP-processed high-purity aluminium from [16]. In this latter case, similar grain microstructures were observed already after 4 passes, and also after 8 passes and 12 passes of ECAP, route B_c, respectively. In sum-

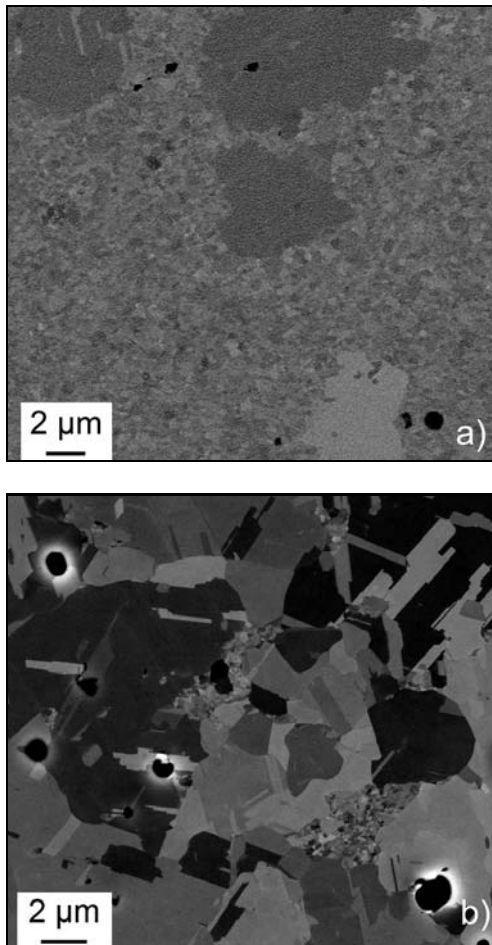


Fig. 7. ECAP-processed commercial purity copper (8 passes, B_c , 5 mm s^{-1}). SEM micrographs of interiors of billets: a) Shortly (2.5 weeks) after ECAP. Some few coarsened grains embedded in original UFG microstructure. From [9]. b) 10 months after ECAP. Strongly coarsened microstructure. Only very few small UFG regions are left over.

mary, the occurrence of bimodal grain size distributions in UFG aluminium (and very probably also in other materials) seems to depend on several factors such as the material, its purity, its SFE, the kind of mechanical stressing and, almost certainly, also on the homologous temperature at which the tests are conducted.

5.2. Evolution of bimodal grain size distributions during or shortly after ECAP

In view of the experience mentioned earlier in Section 4.2, namely that the grain structure in UFG commercial purity copper was found to be bimodal some months after ECAP-processing, an experimental check was made to see whether the grain microstructure exhibited coarsening already shortly after ECAP

and how it changed during subsequent resting at RT. For this purpose, billets of commercial purity copper were subjected to 8 ECAP passes, route B_c , with back pressure, at rather high ECAP deformation rates of 5 mm s^{-1} and 10 mm s^{-1} [9], and inspected after rests of ca. 2.5 weeks and 10 months at RT after ECAP-processing, respectively. Already in the former case, regions with bimodal grain structures could be found [9]. These regions were most marked in the centre of the billet (cross section $20 \text{ mm} \times 20 \text{ mm}$). An example of the locally coarsened grain structure is shown in Fig. 7a. It was concluded that the coarsening observed probably resulted from an *in situ* anneal due to the deformation-induced heating during (rapid) ECAP-processing, being stronger in the centre than at the periphery because of less heat loss. This view is supported by simulations of the heat development during ECAP, as outlined in Section 7. After a rest of 10 months after ECAP processing, the degree of bimodality had progressed markedly. An example is shown in Fig. 7b. It follows from these observations that longer anneals at RT lead to bimodal coarsening, in agreement with earlier experience [8, 9].

6. Exploitation of bimodal grain size distributions to enhance monotonic and fatigue strength

As already discussed, beneficial effects of bimodal grain size distributions have been noted in some cases. Shortly after the work of Höppel et al. [11, 12], Ma and his group succeeded in producing copper with an excellent combination of good monotonic strength and ductility by cold rolling at liquid nitrogen temperature, followed by an annealing treatment which again led to a bimodal grain size distribution [25]. Based on this success, Ma and others have since advocated the advantages of using material with a bimodal grain size distribution for obtaining good strength and ductility [25, 26].

However, this expectation is not always borne out in practice. As stated previously, attempts to introduce a bimodally coarsened grain structure in commercial purity UFG aluminium by annealing were not successful. On the other hand, in the case of UFG α -brass, a bimodal grain size distribution was introduced successfully by annealing [6]. Nonetheless, and in spite of systematic variation of the parameters of the annealing treatment, only a marginal improvement of the fatigue performance was achieved [6, 9]. In a similar vein, attempts to improve the LCF performance of a UFG IF steel (IF: interstitial-free) by introducing a bimodal grain structure by an annealing treatment were unsuccessful [46]. It follows, in accordance with the arguments presented earlier, that the question whether the LCF performance can be enhanced

by introduction of a bimodal grain size distribution by an annealing treatment depends both on the material (SFE, etc.) and also on finding the optimal annealing conditions.

7. Effects of temperature rise during ECAP

It is well known that most of the energy of plastic deformation ($> 90\%$) is dissipated as heat and can lead to a non-negligible temperature rise which can cause microstructural changes. In the case of all SPD processes, the energy of deformation per unit volume $\sigma \cdot \varepsilon$ (σ – stress, ε – strain) is large. Referring to ECAP of a material with a yield stress σ of say 300 MPa and a strain per ECAP pass of $\varepsilon \approx 1$, one obtains $\sigma \cdot \varepsilon \approx 3 \times 10^6 \text{ J m}^{-3}$! With a rather high but typical ECAP speed of some mm s^{-1} , the rate of energy dissipation per unit volume is as large as some 10^5 W m^{-3} ! With regard to the question how seriously the grain size distribution is affected by the heat developed during ECAP, the following different factors are important:

- the maximum temperature attained *locally* in the shear deformation zone during ECAP and
- the time spent *locally* at or near this maximum temperature, and
- the rate of decay of temperature during cooling of the ECAP-processed billet.

In order to assess these effects, experimental and theoretical studies are necessary. First experimental evidence of (adiabatic) temperature rises during ECAP was presented for aluminium and different Al-based alloys [47] and later for some aluminium alloys and a magnesium alloy [48]. In another study, the importance of heating during ECAP with respect to the evolution of the grain structure was discussed [49]. Employing a lumped heat transfer analysis, Kim derived a rather simple analytical expression to estimate the temperature rise in the deformation zone [50] and achieved good agreement with the experimental data reported in [47]. In different finite element modelling (FEM) studies, the temperature distribution in the billet and the temporal evolution of the temperature rise were simulated for aluminium alloys [51, 52] and for steel [51].

Since these studies do not provide results directly applicable to the present work, the temperature rise of copper under ECAP-conditions employed in the laboratory of one of the authors (R. L.) at Monash University has been estimated. Details of these calculations are presented in the Appendix. The computations were performed in three different ways. Finite element modelling (FEM) was applied to simulate the temperature distribution in the billet in the process of ECAP-processing (A1). Next, the simple analytical model derived by Kim [50] was used in order to obtain an estimate of the temperature rise in the shear

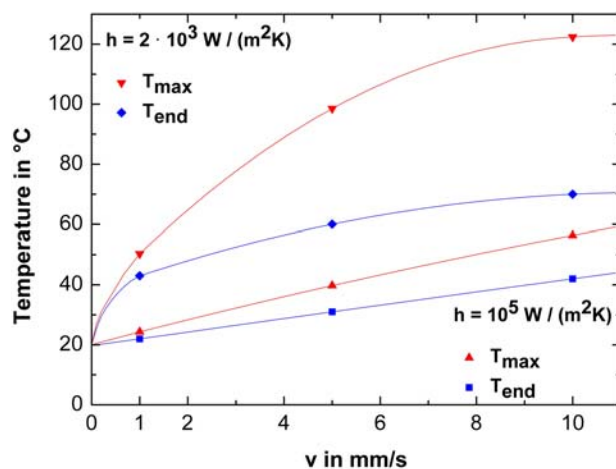


Fig. 8. Summary of results of FEM simulations of maximum temperature T_{\max} in the shear deformation zone and temperature T_{end} at deformed end of billet, plotted as a function of ECAP speed v , for two different values of the heat transfer coefficient ($h = 2 \times 10^3 \text{ W m}^{-2} \text{ K}^{-1}$ and $h = 10^5 \text{ W m}^{-2} \text{ K}^{-1}$).

deformation zone in the bend of the channel in the die (A2). In addition, the decay of the mean temperature averaged over the whole billet after ECAP was described in an approximate analytical model (A3). For further details, the reader is referred to the Appendix. These three attempts to simulate the temperature evolution during and after ECAP have been assessed in a more detailed study [53].

Here, only the main results and conclusions will be presented. The accuracy of the estimates depends on some assumptions. In particular, the value of the heat transfer coefficient used, compare [50, 51, 54, 55], is critical. Figure 8 summarizes the results of the FEM simulations of the maximum temperatures T_{\max} which develop in the main shear deformation zone in the bend of the channel in the ECAP die, plotted as a function of ECAP speed v . In addition, the temperatures T_{end} at the deformed and already slightly cooled end of the billet are also plotted in the figure. The FEM simulations had been conducted for 3 different heat transfer coefficients h ($2 \times 10^3 \text{ W m}^{-2} \text{ K}^{-1}$, $20 \times 10^3 \text{ W m}^{-2} \text{ K}^{-1}$ and $10^5 \text{ W m}^{-2} \text{ K}^{-1}$) and for values of $v = 1, 5$ and 10 mm s^{-1} . The figure shows the results obtained for the largest and smallest values of h . The actual values of the temperatures T_{\max} and T_{end} are believed to lie between these limiting curves. As expected, larger temperature rises occur at higher ECAP speeds. Thus, for the ECAP speeds of 1, 5 and 10 mm s^{-1} , typical mean temperature rises ΔT are roughly 25°C, 55°C and 80°C, corresponding to values of $T_{\max} = RT + \Delta T$ of about 45°C, 75°C and 100°C, respectively. The values T_{\max} obtained by the simple analytical model (A2) differ somewhat but fall into the same range. It must be borne in mind

that these maximum temperatures prevail only for a short time during the ECAP deformation. Moreover, it can be shown by a simple analytical estimate that the billet, once deformed, cools rather quickly and attains the temperature T_0 of the surroundings already after about a minute. The annealing effect thus consists of short heating at the maximum temperature for some seconds, followed by annealing at a quickly decreasing lower temperature. However, the temperatures attained are large enough to induce recovery and, depending on the kind and purity of the material and the conditions of ECAP processing, possibly also recrystallization of the heavily pre-deformed UFG microstructure. Hence, *it is concluded that under specific conditions a bimodally coarsened grain structure can develop already during or very shortly after ECAP processing.*

8. Summary and conclusions

Summarizing and confining ourselves to the well investigated cases, the following conclusions are drawn with respect to the factors governing the occurrence of coarsening, the evolution of bimodal grain size distributions and their effects on the mechanical properties:

- Some UFG metals (e.g. copper or nickel) produced by ECAP have a strong tendency to undergo local grain coarsening by dynamic recrystallization and to develop bimodal grain size structures during mild annealing or cyclic deformation at rather low temperature (RT).

- Other UFG materials, e.g. aluminium (rather high SFE) of commercial purity, also exhibit grain growth at RT but in a rather uniform homogeneous manner. On the other hand, experimental evidence indicates that bimodal grain structures can develop in high-purity UFG aluminium.

- Bimodal grain size structures can evolve already during ECAP by *in situ* annealing, due to the heat production and temperature rise, especially at rather high ECAP deformation rates.

- In strain-controlled RT fatigue but much less so in stress-controlled fatigue, bimodal grain size distributions evolve in UFG copper and UFG nickel, accompanied by cyclic softening, but not in commercial purity UFG aluminium.

- Ageing for short times at elevated temperatures or at RT for longer periods (months, years) leads to local grain coarsening and formation of bimodal grain size distributions in some cases (UFG copper, nickel) but not in the case of UFG aluminium of commercial purity.

- Local grain coarsening is expected to be impeded in less pure UFG material. However, bimodal grain size distributions have been found in commercial and high purity materials. It is desirable to obtain

clearer evidence in different ECAP-processed materials at comparable homologous temperatures, in dependence on purity and also SFE.

- Introduction of bimodal grain size distributions by an annealing treatment can enhance the monotonic and fatigue strength properties of UFG materials considerably or only marginally, depending on the annealing conditions and the material.

- Enhancement of mechanical properties by annealing in order to introduce bimodal grain size distributions is not possible in all materials and requires suitable choice of material and “optimal” annealing conditions.

Acknowledgements

The authors thank Prof. H. S. Kim sincerely for his help and for useful advice concerning the correct application of his estimate of the temperature rise during ECAP and for the choice of appropriate heat transfer coefficients. The support of Deutsche Forschungsgemeinschaft (DFG) within the framework of the DFG Research Unit Ultra Fine Grained Materials is acknowledged gratefully by three of the co-authors (M. K., A. B., H. W. H.).

References

- [1] VALIEV, R. Z.—ISLAMGALIEV, R. K.—ALEXANDROV, I. V.: *Progr. Mater. Sci.*, 45, 2000, p. 103. [doi:10.1016/S0079-6425\(99\)00007-9](https://doi.org/10.1016/S0079-6425(99)00007-9)
- [2] FURUKAWA, M.—IWAHASHI, Y.—HORITA, Z.—NEMOTO, M.—LANGDON, T. G.: *Mater. Sci. Eng. A*, 257, 1998, p. 328. [doi:10.1016/S0921-5093\(98\)00750-3](https://doi.org/10.1016/S0921-5093(98)00750-3)
- [3] VALIEV, R. Z.—ESTRIN, Y.—HORITA, Z.—ZEHETBAUER, M. J.—ZHU, Y. T.: *JOM*, 58, 2006, p. 33.
- [4] THIELE, E.—BRETSCHNEIDER, J.—HOLLANG, L.—SCHELL, N.—HOLSTE, C.: In: *Investigations and Applications of Severe Plastic Deformation*. Eds.: Lowe, T. C., Valiev, R. Z. Dordrecht, Kluwer Academic Publishers 2000, p. 173.
- [5] KLEMM, R.—THIELE, E.—HOLLSTE, C.—ECKERT, J.—SCHELL, N.: *Scripta Mater.*, 46, 2002, p. 685. [doi:10.1016/S1359-6462\(02\)00054-4](https://doi.org/10.1016/S1359-6462(02)00054-4)
- [6] MUGHRABI, H.—HÖPPEL, H. W.—KAUTZ, M.—VALIEV, R. Z.: *Z. Metallkd.*, 94, 2003, p. 1079.
- [7] MOLODOVA, X.—GOTTSTEIN, G.—WINNING, M.—HELLMIG, R. J.: *Mater. Sci. Eng., A* 460, 2007, p. 204. [doi:10.1016/j.msea.2007.01.042](https://doi.org/10.1016/j.msea.2007.01.042)
- [8] MISHIN, O. V.—GODFREY, A.: *Met. Mater. Trans. A*, 39, 2008, p. 2923. [doi:10.1007/s11661-008-9658-3](https://doi.org/10.1007/s11661-008-9658-3)
- [9] HÖPPEL, H. W.—KORN, M.—LAPOVOK, R.—MUGHRABI, H.: In: *Proceedings of 15th Int. Conf. on the Strength of Metals and Alloys (ICSMA 15)*, 2009. Open Access Journal of Physics: Conference Series (JPCS) 2010.
- [10] AGNEW, S. R.—WEERTMAN, J.: *Mater. Sci. Eng. A*, 244, 1998, p. 145. [doi:10.1016/S0921-5093\(97\)00689-8](https://doi.org/10.1016/S0921-5093(97)00689-8)

- [11] HÖPPEL, H. W.—BRUNNBAUER, M.—MUGHRABI, H.—VALIEV, R. Z.—ZHILYAEV, A. P.: In: Proceedings of Materialsweek 2000, <http://www.materialsweek.org/proceedings>, Munich, 2001.
- [12] HÖPPEL, H. W.—ZHOU, Z. M.—MUGHRABI, H.—VALIEV, R. Z.: *Phil. Mag. A*, 82, 2002, p. 1781.
- [13] THIELE, E.—HOLSTE, E.—KLEMM, R.: *Z. Metallkd.*, 93, 2002 p. 730.
- [14] ZHANG, K.—WEERTMAN, J.: *Met. Mater. Trans. A*, 40, 2009, p. 2255. [doi:10.1007/s11661-009-9925-y](https://doi.org/10.1007/s11661-009-9925-y)
- [15] RABKIN, E.—GUTMAN, I.—KAZAKEVICH, M.—BUCHMAN, E.—GORNI, D.: *Mater. Sci. Eng. A*, 396, 2005, p. 11. [doi:10.1016/j.msea.2005.01.015](https://doi.org/10.1016/j.msea.2005.01.015)
- [16] MAY, J.: Mikrostruktur, monotone und zyklische mechanische Eigenschaften ultrafeinkörniger Aluminiumlegierungen. [Doctoral Thesis]. University of Erlangen-Nürnberg, 2008.
- [17] KAWASAKI, M.—HORITA, Z.—LANGDON, T. G.: *Mater. Sci. Eng. A*, 524, 2009, p. 143. [doi:10.1016/j.msea.2009.06.032](https://doi.org/10.1016/j.msea.2009.06.032)
- [18] KWAN, C. C. F.—WANG, Z.: In: Proceedings of FATIGUE 2010. Elsevier, Procedia Engineering, 2, 2010, p. 101.
- [19] ZHANG, K.—WEERTMAN, J.—EASTMAN, J. A.: *Applied Phys. Letters*, 87, 2005, p. 062921-1.
- [20] LEGROS, M.—GIANOLA, D. S.—HEMKER, K. J.: *Acta Mater.*, 56, 2008, p. 3380. PMID:20019286, [doi:10.1016/j.actamat.2008.03.032](https://doi.org/10.1016/j.actamat.2008.03.032)
- [21] RUPERT, T. J.—GIANOLA, D. S.—GAN, Y.—HEMKER, K. J.: *Science*, 326, 2009, p. 1686. [doi:10.1126/science.1178226](https://doi.org/10.1126/science.1178226)
- [22] PATLAN, Y.—VINOGRADOV, A.—HIGASHI, K.—KITAGAWA, K.: *Mater. Sci. Eng. A*, 300, 2001, p. 171. [doi:10.1016/S0921-5093\(00\)01682-8](https://doi.org/10.1016/S0921-5093(00)01682-8)
- [23] HÖPPEL, H. W.—VALIEV, R. Z.: *Z. Metallkd.*, 93, 2002, p. 641.
- [24] MUGHRABI, H.—HÖPPEL, H. W.: *Int. J. Fatigue*, 32, 2010, p. 1413. PMID:12410306, [doi:10.1016/j.ijfatigue.2009.10.007](https://doi.org/10.1016/j.ijfatigue.2009.10.007)
- [25] WANG, Y.—CHEN, M.—ZHOU, F.—MA, E.: *Nature*, 419, 2002, p. 912. [doi:10.1038/nature01133](https://doi.org/10.1038/nature01133)
- [26] MA, E.: *Scripta Mater.*, 49, 2003, p. 663.
- [27] LEE, Z.—WITKIN, D. B.—RADMILOVIC, V.—LAVERNIA, E. J.—NUTT, S. R.: *Mater. Sci. Eng. A*, 410–411, 2005, p. 462. [doi:10.1016/j.msea.2005.08.104](https://doi.org/10.1016/j.msea.2005.08.104)
- [28] LEE, Z.—RADMILOVIC, V.—AHN, B.—LAVERNIA, E. J.—NUTT, S. R.: *Met. Mater. Trans. A*, 41, 2010, p. 795. [doi:10.1007/s11661-009-0007-y](https://doi.org/10.1007/s11661-009-0007-y)
- [29] WINNING, M.—GOTTSTEIN, G.—SHVINDLERMANN, L. S.: *Mater. Sci. Eng. A*, 317, 2001, p. 17. [doi:10.1016/S0921-5093\(01\)01193-5](https://doi.org/10.1016/S0921-5093(01)01193-5)
- [30] LUKÁŠ, P.—KUNZ, L.—SVOBODA, M.: *Mater. Sci. Eng. A*, 391, 2005, p. 337.
- [31] KUNZ, L.—LUKÁŠ, P.: private communication, 2009.
- [32] AGNEW, S. R.—VINOGRADOV, A. YU.—HASHIMOTO, S.—WEERTMAN, J. R.: *J. of Electronic Materials*, 28, 1999, p. 1038. [doi:10.1007/s11664-999-0181-0](https://doi.org/10.1007/s11664-999-0181-0)
- [33] MUGHRABI, H.—HÖPPEL, H. W.: *Mater. Res. Soc. Symp. Proc.*, B2.1.1–B2.1.12, 2001, p. 634.
- [34] MORROW, J. D.: In: Internal friction, damping and cyclic plasticity. ASTM STP 378, 1965, p. 45.
- [35] LANDGRAF, R. W.: In: Achievement of high fracture resistance in metals and alloys. ASTM STP 467, 1970, p. 3.
- [36] HÖPPEL, H. W.: *Mater. Sci. Forum*, 503–504, 2006, p. 259. [doi:10.4028/www.scientific.net/MSF.503-504.259](https://doi.org/10.4028/www.scientific.net/MSF.503-504.259)
- [37] MUGHRABI, H.: In: Investigations and Applications of Severe Plastic Deformation. Eds. Lowe, T. C., Valiev, R. Z. Dordrecht, Kluwer Academic Publishers 2000, p. 241.
- [38] MUGHRABI, H.—HÖPPEL, H. W.—KAUTZ, M.: *Scripta Mater.*, 51, 2004, p. 807. [doi:10.1016/j.scriptamat.2004.05.012](https://doi.org/10.1016/j.scriptamat.2004.05.012)
- [39] HÖPPEL, H. W.—KAUTZ, M.—MURASHKIN, M.—LANGDON, T. G.—VALIEV, R. Z.: *Int. J. Fatigue*, 28, 2005, p. 1.
- [40] HÖPPEL, H. W.—VINOGRADOV, A.—MUGHRABI, H.: In: Bulk nanostructured materials. Eds.: Zehetbauer, M. J., Zhu, Y. T. Weinheim, WILEY-VCH 2009, p. 481.
- [41] LAPOVOK, R.: *J. Mater. Sci.*, 40, 2005, p. 341. [doi:10.1007/s10853-005-6088-0](https://doi.org/10.1007/s10853-005-6088-0)
- [42] MUGHRABI, H.—WANG, R.: In: Basic Mechanisms in Fatigue of Metals. Eds.: Lukáš, P., Polák, J. Amsterdam, Elsevier 1988, p. 1.
- [43] VALIEV, R. Z.—ALEXANDROV, I. V.—ZHU, Y. T.—LOWE, T. C.: *J. Mater. Research*, 17, 2002, p. 5.
- [44] STÜWE, H. P.—PADILHA, A. F.—SICILIANO, F., Jr.: *Mater. Sci. Eng. A*, 333, 2002, p. 361.
- [45] ORLOV, D.—TODAKA, Y.—UMEMOTO, M.—TSUJI, N.: in preparation.
- [46] NIENDORF, T.—CANADINC, D.—MAIER, H. J.—KARAMAN, I.: *Int. J. Fatigue*, 30, 2008, p. 426. [doi:10.1016/j.ijfatigue.2007.04.015](https://doi.org/10.1016/j.ijfatigue.2007.04.015)
- [47] YAMAGUCHI, D.—HORITA, Z.—NEMOTO, M.—LANGDON, T. G.: *Scripta Mater.*, 41, 1999, p. 791. [doi:10.1016/S1359-6462\(99\)00233-X](https://doi.org/10.1016/S1359-6462(99)00233-X)
- [48] SEMIATIN, S. L.—BERBON, P. B.—LANGDON, T. G.: *Scripta Mater.*, 44, 2001, p. 135. [doi:10.1016/S1359-6462\(00\)00565-0](https://doi.org/10.1016/S1359-6462(00)00565-0)
- [49] NISHIDA, Y.—ANDO, T.—NAGASE, M.—LIM, S.—SHIGEMATSU, I.—WATAZU, A.: *Scripta Mater.*, 46, 2002, p. 211. [doi:10.1016/S1359-6462\(01\)01226-X](https://doi.org/10.1016/S1359-6462(01)01226-X)
- [50] KIM, H. S.: *Scripta Mater.*, 42, 2001, p. 536.
- [51] PEL, Q. X.—HU, B. H.—LU, C.—WANG, Y. Y.: *Scripta Mater.*, 49, 2003, p. 303. [doi:10.1016/S1359-6462\(03\)00284-7](https://doi.org/10.1016/S1359-6462(03)00284-7)
- [52] QUANG, P.—KRISHNAIAH, A.—HONG, S. I.—KIM, H. S.: *Materials Transactions*, 50, 2009, p. 40. [doi:10.2320/matertrans.MD200823](https://doi.org/10.2320/matertrans.MD200823)
- [53] LAPOVOK, R.—MUGHRABI, H.: unpublished.
- [54] LENHAR, A. L., Jr.—DAMASIO, S. F.—MILKE, A. R.—SCHAEFFER, L.: In: Proceedings of 4th JSTP International Seminar on Precision Forging 2006. Eds.: Kitamura, K., Matsumoto, R. Tokyo, The Japan Society for Technology of Plasticity 2006, p. 93.
- [55] KANG, J. H.—LEE, K. O.—KANG, S. S.: *J. Achievements in Materials and Manufacturing Engineering*, 20, 2007, p. 367.

Appendix

Temperature rise during ECAP

During severe plastic deformation by a process such as ECAP, an appreciable amount of energy of deformation is dissipated in relatively short time, leading to a non-negligible temperature rise that can cause microstructural changes. Here, estimates of the temperature rise, obtained by different approaches, will be presented and discussed.

A1. Finite element simulation

Finite Element (FEM) modelling of the ECAP deformation process was performed for the geometry of the ECAP die used at Monash University (square cross section of the channel, edge length $q = 20$ mm) and for billets of dimension $q \times q \times l = 20$ mm \times 20 mm \times 120 mm. The commercial package Q-Form was used which is designed particularly to model forging and extrusion [A1] and which is widely used in the metal forming industry because of its accuracy and effectiveness, as was demonstrated by the benchmark test at the International Conference on “Metal Forming Process Simulation in Industry” [A2]. The Q-Form system is based on flow formulation which relates the stresses to the plastic strain increments and the material is treated as an incompressible rigid-viscoplastic continuum. The system provides coupled thermo-mechanical interactive simulation of metal flow, where the flow stress is represented as a function of strain, strain rate and temperature in analytical or table form. As the accuracy of the numerical simulation strictly depends on the input data, the data on flow stress of copper should be introduced into the FE package as a function of strain, strain rate and temperature. However, in the present case, a single stress-strain curve from a room temperature test was taken as input data. This would be correct for the first ECAP pass for annealed material. For later ECAP passes, it would be more appropriate to use the (constant) value of the yield stress that is attained after a few passes. The physical properties used in the simulation were as follows: density $\rho = 8940$ kg m $^{-3}$; thermal conductivity $k = 401$ W m $^{-1}$ K $^{-1}$; specific heat $C = 385$ J kg $^{-1}$ K $^{-1}$. The lubricant was taken as ideal with coefficient of friction equal to zero. Neglect of friction implies that the temperature rise will be underestimated by a small amount, as shown in Section A2. The simulations were performed for 3 different values of the effective heat transfer coefficient from the workpiece to the die through a lubricant layer, namely 2×10^3 W m $^{-2}$ K $^{-1}$, 20×10^3 W m $^{-2}$ K $^{-1}$ and 10^5 W m $^{-2}$ K $^{-1}$. The temperature rise was com-

puted for three different ECAP speeds, namely 1, 5 and 10 mm s $^{-1}$.

Figure A1 shows examples of the distribution of the absolute temperature (referred to room temperature RT of 20°C) in the partially deformed workpiece in the channel of the ECAP die. In all cases, it is impressively shown that the highest value of the local temperature, T_{\max} , develops in the shear deformation zone at the bend of the channel. The comparison of Figs. A1a,b for ECAP speeds of 1 mm s $^{-1}$ and 10 mm s $^{-1}$, respectively, computed with $h = 20 \times 10^3$ W m $^{-2}$ K $^{-1}$, shows that the temperature rise is significantly larger at higher ECAP speed. Figures A2a,b refer to the same ECAP speed of 5 mm s $^{-1}$, but to simulations with $h = 2 \times 10^3$ W m $^{-2}$ K $^{-1}$ and $h = 10^5$ W m $^{-2}$ K $^{-1}$, respectively. In the latter case, when the larger value of the heat transfer coefficient is used in the simulation, the temperature rise ΔT (difference between T_{\max} and 20°C) obtained is markedly lower, namely 19.73°C instead of 78.52°C, when the lower value of h is used. It is thus obvious that the absolute values of the temperatures obtained in the FE simulation depend sensitively on the heat transfer from the workpiece through the lubricant to the die. The dependence on ECAP speed v is summarized in Fig. 8, showing the maximum local temperature T_{\max} in the deformation zone as a function of ECAP speed v . The temperatures T_{end} at the deformed end of the ECAP-processed workpiece at a distance of about 100 mm from the deformation zone are also plotted. This gives an impression of the temperatures at a location of the workpiece after ECAP processing at the speeds of 10 mm s $^{-1}$ and 1 mm s $^{-1}$, and after having cooled down for times of ca. 10 s or ca. 100 s, respectively.

A2. Analytical estimate of temperature rise ΔT in shear deformation zone

Kim has derived the following rather simple formula to estimate under plausible assumptions the temperature rise ΔT in the shear deformation zone [50]:

$$\Delta T = \frac{0.9\sigma\varepsilon + 0.5m(\sigma/\sqrt{3})v\frac{A}{V}\Delta t}{\rho C + \frac{A}{V}h\Delta t}, \quad (\text{A1})$$

where σ is the yield stress of the material and ε the strain attained during one ECAP pass, v is the ECAP speed, A is the outer area of the shear deformation zone, V is its volume, Δt is the passing time through the shear deformation zone (where Δt is directly proportional to the die corner angle Ψ) and m is the coefficient of friction, taken as 0.2 [50]; h , C and ρ

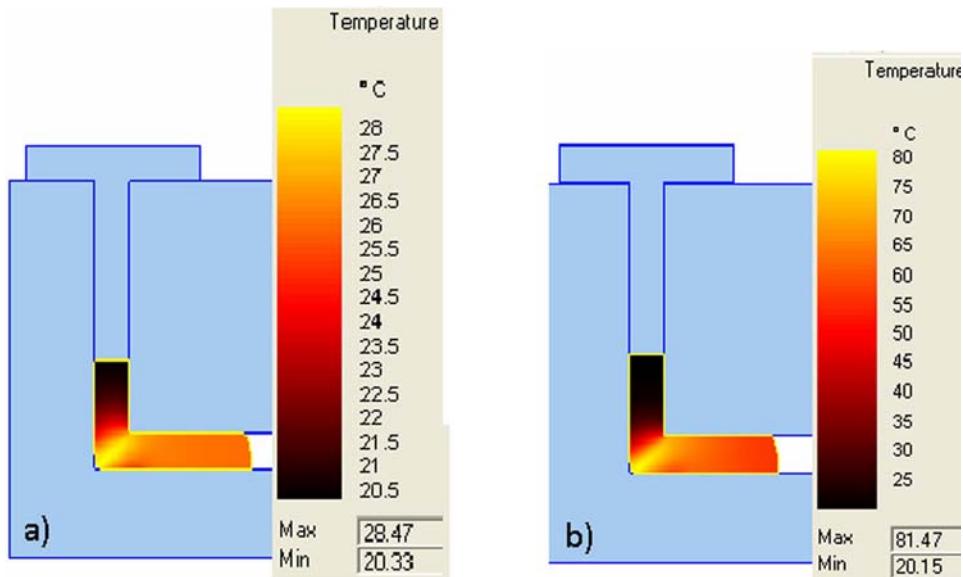


Fig. A1. FEM simulation of temperature distribution in billet during ECAP, computed with $h = 2 \times 10^3 \text{ W m}^{-2} \text{ K}^{-1}$, showing effect of ECAP speed v . a) $v = 1 \text{ mm s}^{-1}$, b) $v = 10 \text{ mm s}^{-1}$.

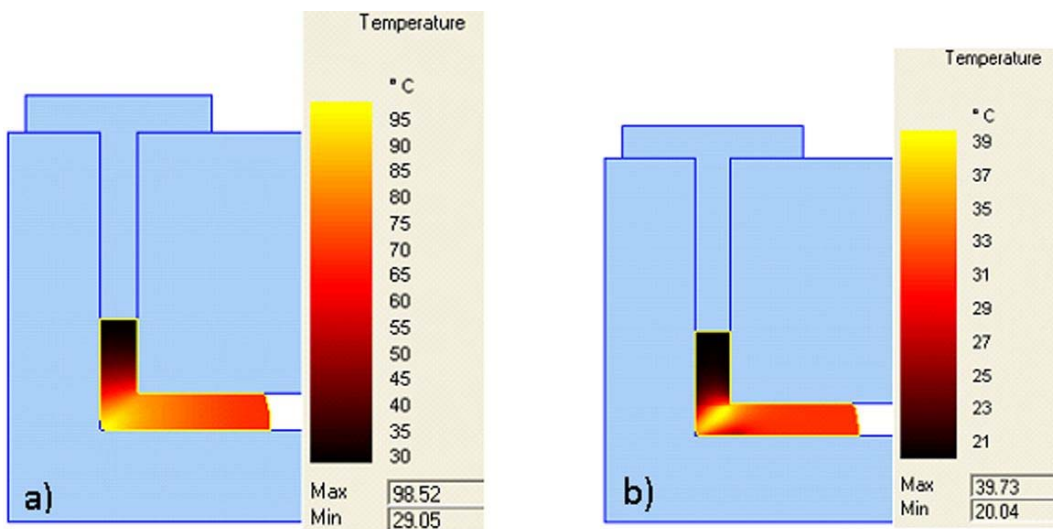


Fig. A2. FEM simulation of temperature distribution in billet during ECAP, computed for ECAP speed of $v = 5 \text{ mm s}^{-1}$, showing effect of different values of heat transfer coefficient h . a) $h = 2 \times 10^3 \text{ W m}^{-2} \text{ K}^{-1}$, b) $h = 10^5 \text{ W m}^{-2} \text{ K}^{-1}$.

have the same meanings as before. Using this simple analytical expression, with A and V estimated for a die corner angle Ψ of 45° as stated in [48], and with $h = 2 \times 10^3 \text{ W m}^{-2} \text{ K}^{-1}$, Kim obtained very satisfactory agreement between computed values of ΔT and the experimental results obtained by Yamaguchi et al. [47] in the case of ECAP-processed Al and Al-Mg alloys for different values of v . It follows from a comparison of the first and the second term in the numerator of Eq. (A1) that the main contribution to ΔT comes from the work of deformation and that the heat of friction is almost negligible.

The same procedure was applied to estimate the

temperature rise ΔT in the case of a copper billet. Assuming a yield stress of 350 MPa (typical of UFG copper [1]) and a typical value of $\varepsilon \approx 1$, then with the same values of 45° for the die corner angle Ψ (estimated also from the FEM plots), $m = 0.2$ and $h = 2 \times 10^3 \text{ W m}^{-2} \text{ K}^{-1}$ as in the estimate of Kim, and after due consideration of the dimensions of the billet, as stated before, the temperature rise ΔT was estimated as approximately 64°C , 89°C and 94°C , corresponding to values of T_{max} of 84°C , 109°C and 114°C , for ECAP speeds of 1 mm s^{-1} , 5 mm s^{-1} and 10 mm s^{-1} , respectively. These values can be compared with the values of T_{max} obtained by FEM for

$h = 2 \times 10^3 \text{ W m}^{-2} \text{ K}^{-1}$, as shown in Fig. 8, and are found to lie in the same range, being however slightly lower at the higher ECAP speed and significantly higher at the lower ECAP speed than the values obtained by FEM. It is suggested that there are several reasons for these discrepancies: a) the FEM simulations refer to the temperature distribution in the whole billet, whereas Eq. (7) represents only an approximate estimate of the temperature rise in the shear deformation zone, and b) there is an uncertainty in the assessment of realistic values of the passing time Δt in formula (A1), which is essentially defined via the die corner angle Ψ [50]. If so, then the deviations from the FEM results could imply that the die corner angle Ψ depends on the ECAP speed v and is apparently somewhat larger at lower ECAP speeds. A more detailed study would be necessary to check whether this reasoning is correct.

A3. Simple estimate of decay of mean temperature $T(t)$ in billet after ECAP

It is difficult to derive in simple terms an analytical solution describing the differential temporal change of the mean temperature $T(t)$ of a billet deformed by ECAP as a function of time t . However, the decay of the mean temperature T of the billet immediately after one ECAP pass can be estimated in a rather simple manner to yield information complementary to the FEM simulation of the local temperature evolution during ECAP and the simple analytical estimate of the temperature achieved in the shear deformation zone.

A simple estimate shows that the heat capacity of the steel die is usually much larger than that of a copper billet. Hence, the temperature T_0 of the surroundings will remain approximately constant, while the billet is heated during ECAP. Next, assuming sufficiently fast heat conduction in the billet, it can be expected that shortly after completion of an ECAP pass a more or less homogeneous temperature distribution will be attained, with a mean temperature T over the whole billet length. The subsequent cooling

rate can then be expressed as

$$\left(\frac{dT}{dt}\right)_{\text{cool}} = -\frac{hA}{\rho CV}(T - T_0) = -B(T - T_0), \quad (\text{A2})$$

where A now is the total area of the billet which is in touch with the walls of the channel ($A = 4lq$, l is length of billet, q is edge length of square cross section of billet), and V is the volume of the whole billet ($V = lq^2$). Then, integration between the limits of the initial temperature T_{in} and the current temperature $T(t)$ yields

$$T(t) = T_0 + e^{\ln(T_{\text{in}} - T_0) - Bt}. \quad (\text{A3})$$

From the FEM simulations summarized in Fig. 8 and from the preceding simple analytical estimate of the temperature rise in the shear deformation zone, it follows for a heat transfer coefficient of $h = 2 \times 10^3 \text{ W m}^{-2} \text{ K}^{-1}$ (as in Sect. A2, compare [50]) that a typical temperature in the billet shortly after an ECAP pass is in the order of 80°C (corresponding to a rough average between T_{max} and T_{end}). If this value is taken as the initial temperature T_{in} in Eq. (A3), one finds that, after 5 s and 10 s, the mean temperature of the billet has dropped to roughly 53°C and 38°C , respectively. Already after about 35 s, one finds $T \approx T_0 \approx 20^\circ\text{C}$. Thus, the implication is that subsequent cooling following an ECAP pass is fast and that the main effect of heating during ECAP occurs already during the ECAP deformation.

References

- [A1] Q-Form User's Guide. Moscow, Quantor Ltd. 2000.
- [A2] BIBA, N.—LISHNIJ, A.—SADYKHOV, O.—STIEBOUNOV, S.: In: Proceedings of the International Conference and Workshop on Metal Forming Simulation in Industry. Vol. 2. Wuppertal, Germany, Werner Fastenrath Druckerei 1994, p. 302. ISBN 3930683288